The Effect of Yarkovsky Thermal Forces on the Dynamical Evolution of Asteroids and Meteoroids

William F. Bottke Jr.
Southwest Research Institute

David Vokrouhlický
Charles University, Prague

David P. Rubincam
NASA Goddard Space Flight Center

Miroslav Brož
Charles University, Prague

The Yarkovsky effect is a thermal radiation force that causes objects to undergo semimajor axis drift and spinup/spindown as a function of their spin, orbit, and material properties. This mechanism can be used to (1) deliver asteroids (and meteoroids) with diameter D < 20 km from their parent bodies in the main belt to chaotic resonance zones capable of transporting this material to Earth-crossing orbits, (2) disperse asteroid families, with drifting bodies jumping or becoming trapped in mean-motion and secular resonances within the main belt, and (3) modify the rotation rates of asteroids a few kilometers in diameter or smaller enough to possibly explain the excessive number of very fast and very slow rotators among the small asteroids. Accordingly, we suggest that nongravitational forces, which produce small but meaningful effects on asteroid orbits and rotation rates over long timescales, should now be considered as important as collisions and gravitational perturbations to our overall understanding of asteroid evolution.

1. CLASSICAL MODEL OF ASTEROID EVOLUTION

Over the last several decades, it has been assumed that collisions and gravitational forces are the primary mechanisms governing the evolution of asteroids and meteoroids. Using these processes, it is possible to construct an approximate history of how the main-belt and inner solar system asteroid populations have changed over the last several billion years. The main tenets of this model, which we broadly refer to as the "classical" asteroid evolution model, are summarized below.

Asteroids, whose orbits intersect in the main belt, occasionally collide with one another at high velocities (~5 km s^{-1}; *Bottke et al.,* 1994). These events result in cratering and fragmentation, with the collisional physics determining the orbits, spin states, shapes, and internal structures of the surviving bodies. The largest impact events are believed to produce the observed asteroid families. The orbital positions of family members suggest that some ejecta can be launched approximately several 100 m s^{-1} (*Zappalà et al.,* 1996). If true, it is plausible that fragments from asteroid collisions, thrown with just the right trajectory and velocity, can be directly injected into powerful or diffusive resonance zones produced by the gravitational perturbations of the planets (*Farinella et al.,* 1993). Numerical studies have shown that test objects in such resonance regions frequently have their eccentricities pumped up to planet-crossing orbits (e.g., *Wisdom,* 1983). Once on planet-crossing orbits, asteroids have their dynamical evolution dominated by resonances and gravitational close encounters with the planets. Some of these asteroids go on to strike the planets, although most impact the Sun or are ejected from the inner solar system via a close encounter with Jupiter (*Gladman et al.,* 1997). If the object is small, it may also be removed via a catastrophic collision. It is believed that most meteorites and near-Earth asteroids are delivered to the inner solar system (and Earth) by this long chain of events.

Up to now, the classical model (CM) has been useful in helping us interpret asteroid data and broadly understand the evolution of asteroid populations. Nevertheless, some predictions are inconsistent with observations. For example:

CM Prediction 1: Since fresh ejecta is directly injected into chaotic resonances, and the dynamical lifetime of bodies placed in powerful resonances are generally a few million years or less (*Gladman et al.,* 1997), we should expect to see an abundance of meteorites with short cosmic-ray-exposure (CRE) ages (i.e., only a few million years) and a paucity of long-lived meteorites.

Observation 1: Relatively few meteorites have CRE ages less than ~10 m.y. Most stony meteorites have CRE ages between ~10 and 100 m.y., while iron meteorites have CRE ages between ~0.1 and 1.0 G.y. (*Caffee et al.,* 1988; *Marti and Graf,* 1992). In general, CRE ages are compa-

rable to, or longer than, the average dynamical lifetime of Earth-crossing asteroids (~10 m.y.; *Gladman et al.,* 1997; *Migliorini et al.,* 1997; *Morbidelli and Gladman,* 1998).

CM Prediction 2: There are roughly 5000–6000 kilometer-sized asteroids crossing the orbits of the terrestrial planets (*Bottke et al.,* 2001a). These bodies have a wide range of taxonomic types (e.g., *Binzel et al.,* 2001). To keep this population in steady state, disruption events among large, spectrally diverse asteroids must be frequent, particularly since these are the only events capable of injecting kilometer-sized fragments into suitable resonant "escape hatches." Since most of these asteroids come from the inner and central main belt (*Bottke et al.,* 2001a), we should expect these regions to contain numerous asteroid families. Moreover, since the planet-crossing asteroids are "fresh ejecta," they should have a relatively steep size-frequency distribution.

Observation 2: Few asteroid families can be found in the inner and central main belt, while most potential parent asteroids for the kilometer-sized inner solar system asteroids reside in dynamically stable regions far from resonant "escape hatches." Modeling results including these constraints suggest that the direct injection of asteroid fragments into resonances is too inefficient to keep the inner solar system asteroid population in steady state (*Zappalà and Cellino,* 2002). In addition, the size-frequency distribution of kilometer-sized near-Earth objects (NEOs) is fairly shallow (*Bottke et al.,* 2000a).

CM Prediction 3: Studies of asteroid families suggest that many large fragments are ejected from the impact site at high velocities (approximately several 100 m s^{-1}), with the smallest fragments traveling the furthest from the cluster center (*Cellino et al.,* 1999).

Observation 3: The peak velocities of size-velocity distributions derived from numerical hydrocode results are generally much lower than those inferred from the orbital positions of asteroid family members (*Pisani et al.,* 1999). Though it is possible that hydrocodes are inaccurate, they have successfully reproduced results ranging from laboratory impact experiments, where centimeter-sized projectiles are shot into targets, to underground nuclear explosions (e.g., *Benz and Asphaug,* 1999).

CM Prediction 4: Asteroid collisions should produce a wide range of asteroid spin rates. To zeroth order, we would expect the spin rates for large and small asteroids to follow a Maxwellian frequency distribution (e.g., *Binzel et al.,* 1989; *Davis et al.,* 1989).

Observation 4: The distribution of spin rates among observed small asteroids (D < 10 km) contains an excess number of fast rotators and very slow rotators when this data is fit to Maxwellian distribution (*Pravec and Harris,* 2000; *Pravec et al.,* 2002).

We believe there is a connection between these mismatches, and that an important physical mechanism is missing from the classical model, namely how nongravitational forces affect the evolution of asteroids. It is already well known that the dynamical evolution of dust particles can be explained using Poynting-Robertson drag, a radiation effect that causes small objects to spiral inward as they absorb energy and momentum streaming radially outward from the Sun and then reradiate this energy isotropically in their own reference frame (e.g., *Burns et al.,* 1979; *Dermott et al.,* 2002). It is not as well known, however, that a different nongravitational force called the Yarkovsky effect can compel objects between 0.1 m and 20 km to spiral inward or outward at different rates as a function of their spin, orbit, and material properties, or that a variant of this force can also modify the spin rates of asteroids. As we will show in this chapter, this previously known but mostly ignored effect, which can be essentially described as a radiation recoil produced by asymmetrically reradiated thermal energy, has the potential to resolve many of the problems described above. Accordingly, we believe the classical model should now be revised to include nongravitational forces as a third important mechanism, in addition to gravity and collisions, affecting asteroid evolution.

2. INTRODUCTION TO THE YARKOVSKY EFFECT

Ivan Osipovich Yarkovsky (1844–1902), a civil engineer who worked on scientific problems in his spare time, first proposed the effect that now bears his name (*Neiman et al.,* 1965). Writing in a pamphlet around the year 1900, Yarkovsky noted that the diurnal heating of a rotating object in space would cause it to experience a force that, while tiny, could lead to large secular effects in the orbits of small bodies, especially meteoroids and small asteroids (*Öpik,* 1951). Yarkovsky's effect is a radiation force, and is the photonic equivalent of *Whipple*'s (1950) rocket effect.

Yarkovsky's remarkable insight would have been consigned to oblivion had it not been for the brilliant Estonian astronomer Ernst J. Öpik (1893–1985), who read Yarkovsky's pamphlet sometime around 1909. Decades later Öpik, recalling the pamphlet from memory, discussed the possible importance of the Yarkovsky effect for moving meteoroids about the solar system (*Öpik,* 1951). [Curiously, *Öpik*'s (1976) book, which continues the theme of his 1951 paper, makes no mention of Yarkovsky.] Following Öpik and before its current flowering, research on the Yarkovsky-type effect was pursued in Russia by *Radzievskii* (1952, 1954) and *Katasev and Kulikova* (1980); in the United States by *Paddack* (1969, 1973), *Paddack and Rhee* (1975), *Peterson* (1976), *O'Keefe* (1976), *Slabinski* (1977), *Dohnanyi* (1978), and *Burns et al.* (1979); and in Australia by *Olsson-Steel* (1986, 1987). Additional history can be found in *Hartmann et al.* (1999).

2.1. Description of Diurnal Component

The basic idea behind Yarkovsky's diurnal effect is shown in Fig. 1a, which shows a spherical meteoroid in a circular orbit about the Sun. For simplicity, the meteoroid's spin axis is taken to be normal to the orbital plane, so that the Sun always stands on its equator. Insolation heats up the sunward side, with the heat ultimately reradiated into space by the meteoroid (typically in the infrared part of the spectrum,

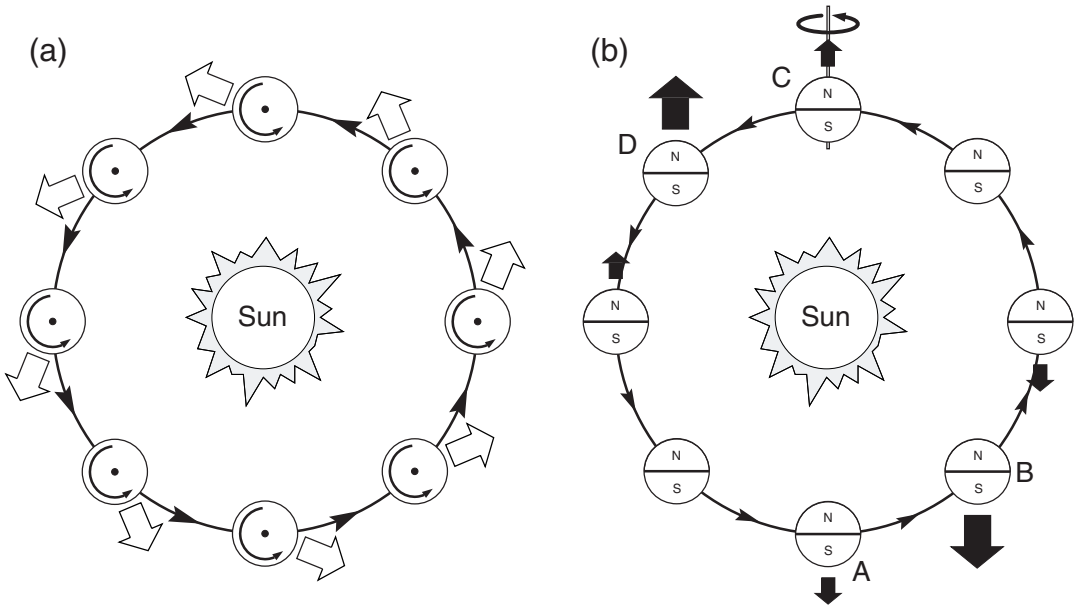

Fig. 1. **(a)** The diurnal Yarkovsky effect, with the asteroid's spin axis perpendicular to the orbital plane. A fraction of the solar insolation is absorbed only to later be radiated away, yielding a net thermal force in the direction of the wide arrows. Since thermal reradiation in this example is concentrated at about 2:00 p.m. on the spinning asteroid, the radiation recoil force is always oriented at about 2:00 a.m. Thus, the along-track component causes the object to spiral outward. Retrograde rotation would cause the orbit to spiral inward. **(b)** The seasonal Yarkovsky effect, with the asteroid's spin axis in the orbital plane. Seasonal heating and cooling of the "northern" and "southern" hemispheres give rise to a thermal force that lies along the spin axis. The strength of the reradiation force varies along the orbit as a result of thermal inertia; even though the maximum sunlight on each hemisphere occurs as A and C, the maximum resultant radiative forces are applied to the body at B and D. The net effect over one revolution always causes the object to spiral inward.

unless the meteoroid is very close to the Sun). An infrared photon carries away momentum when it leaves the meteoroid according to the relation p = E/c, where p is the photon's momentum, E its energy, and c is the speed of light. Because more energy and therefore more momentum departs from the hotter part of the meteoroid than the colder, the meteoroid feels a net kick in the direction away from the hotter part.

If the meteoroid had no thermal inertia, then the temperature distribution would be symmetrical about the subsolar point and the meteoroid would experience a net force radially outward from the Sun. The only consequence of this force would be to weaken the Sun's grip on the meteoroid. However, all bodies have thermal inertia, which causes a delay, so that the hottest part of the meteoroid is its afternoon side rather than the subsolar point. This is similar to the Earth, where the afternoon is typically the warmest time of day. As a result, the force on the meteoroid has not only a component that is radially outward from the Sun, but also has an along-track component.

This along-track component causes a secular increase in the semimajor axis (and, to a lesser degree, eccentricity) for the prograde sense of rotation shown in the figure, so that over time the tiny Yarkovsky force can profoundly change the orbit. The sign of the diurnal Yarkovsky effect depends on the sense of rotation. If the meteoroid shown in Fig. 1a rotated in the retrograde sense, the orbit would shrink instead of expand, while if the rotation axis was in the orbital plane, the diurnal Yarkovsky would be shut off entirely. The magnitude of the diurnal effect also depends on how close a body is to the Sun, the tilt of the body's spin axis with respect to the orbital plane, and the body's physical characteristics (i.e., the size of the body, its shape and thermal properties, and how fast it is rotating). The interplay of these factors means that there is an optimal size for maximizing the diurnal Yarkovsky effect for a given rotation speed and thermal structure. A very large object would have a poor area-to-mass ratio (e.g., the effect is negligible on a large body like the Earth). On the other hand, the smaller the body, the better the area-to-mass ratio, but at some point the radius becomes so small that the thermal wave penetrates all the way across the body, lessening the temperature differences between the night and day sides and weakening the effect (e.g., a slowly rotating dust particle). For rotation periods believed to be typical in the solar system [P ~ 5 h × (D/1 km), where D is the diameter of the body], optimal sizes for the Yarkovsky effect range from centimeters to meters. Objects having zero or infinitely fast rotation rates experience no diurnal Yarkovsky force.

2.2. Description of Seasonal Component

Nearly a century after Yarkovsky wrote his pamphlet, a second Yarkovsky effect emerged. While searching for the

cause of the secular decay of the orbit of the LAGEOS satellite, it was realized that there had to be a seasonal effect (*Rubincam,* 1987, 1988, 1990) in addition to Yarkovsky's original diurnal effect. The seasonal effect applies not just to Earth satellites like LAGEOS, but also to objects orbiting the Sun.

The seasonal Yarkovsky effect is illustrated in Fig. 1b. As in Fig. 1a, a spherical meteoroid is assumed to be in a circular orbit about the Sun; but in this case the spin axis lies in the orbital plane. It is the component of force lying along the spin axis that gives rise to the seasonal effect. When the meteoroid is at A (bottom of the figure) the Sun shines most strongly on its northern hemisphere. As with the diurnal effect, there is a delay due to thermal inertia, so that the northern hemisphere is hottest at B. Likewise, the Sun shines most strongly on the southern hemisphere at C but this hemisphere becomes hottest at D. When the along-track force is averaged around the orbit, it turns out to be nonzero. For a body without thermal inertia, however, the along-track force averages to zero when integrated over one revolution about the Sun.

For small orbital eccentricities, the average along-track force is always in opposition to the motion of the meteoroid. Hence in the small eccentricity regime the seasonal force always acts like drag and causes orbital decay; for this reason the seasonal Yarkovsky effect was originally dubbed "thermal drag" (*Rubincam,* 1987). Unlike the diurnal Yarkovsky effect, the seasonal Yarkovsky effect is independent of the sense of rotation of the meteoroid; reversing its spin does not change the effect's sign. Moreover, the relevant timescale for the seasonal effect is the meteoroid's orbital period rather than the usually much quicker rotational period involved in the diurnal effect.

The seasonal effect does depend on the body's proximity to the Sun and on the tilt of the spin axis with respect to the orbit; it vanishes when the spin axis is normal to the orbital plane. Like in the diurnal case, there is an optimum size for maximizing the effect. For basaltic bodies on circular orbits in the inner main belt, 12-m-diameter objects would experience the greatest effects (*Rubincam,* 1998; *Farinella et al.,* 1998). The seasonal Yarkovsky force also affects the other orbital elements in addition to the semimajor axis. For small eccentricities it tends to circularize the orbit, like atmospheric drag does (*Rubincam,* 1995, 1998; *Vokrouhlický and Farinella,* 1999).

3. THEORY OF THE YARKOVSKY EFFECT

The Yarkovsky force computation naturally splits into two parts: (1) determination of the surface temperature distribution, and (2) evaluation of the thermal radiation recoil force (or torque if desired). Mathematically similar derivations of this solution can be found in several modern references (*Rubincam,* 1995, 1998; *Vokrouhlický,* 1998a,b, 1999; *Vokrouhlický and Farinella,* 1999; *Bottke et al.,* 2000a). In this chapter, we follow the formalism of *Vokrouhlický* (2001).

Problem (1) above has already been examined within the context of asteroid radiometry, but the Yarkovsky application requires some special care. For example, thermal inertia of the surface material — often omitted in radiometry — must now be included. On the other hand, the complexity of the heat diffusion problem can be reduced (within reasonable errors) by adopting linearization (e.g., small temperature differences are referred to a suitably chosen mean value). For simple asteroid shapes, this procedure allows us to compute the Yarkovsky force using analytical expressions. Since most applications of the Yarkovsky effect require rapid computations, it is advantageous to sacrifice some precision for speed. More exact solutions, particularly for irregularly shaped bodies and/or inhomogeneous thermal parameters, require more sophisticated (and computationally expensive) treatments (*Vokrouhlický and Farinella,* 1998, 1999; *Spitale and Greenberg,* 2001, 2002).

To compute the surface temperature on a body, we use the heat diffusion equations for energy flows inside the body

$$\nabla \cdot (K\nabla T) = \rho C \frac{\partial T}{\partial t} \tag{1}$$

or across its surface

$$(K\nabla T \cdot \mathbf{n}_\perp) + \varepsilon\sigma T^4 = \alpha\mathcal{E} \tag{2}$$

the latter of which appears as a boundary condition for the temperature (T) determination. Here, K is the thermal conductivity, C is the specific heat at constant pressure, ρ is the material density, ε is the surface thermal emissivity, σ is the Stefan-Botzmann constant, and $\alpha = 1 - A$, with A being the Bond albedo. Equation (2) refers to a surface element with an external normal vector $\mathbf{n}_\perp$, while $\mathcal{E}$ is the flux of solar radiation through this element. Once the insolation function $\mathcal{E}$ for the surface elements is specified (which requires knowledge of the body's shape and its rotation state) and material parameters (K, C, ρ) are known, equations (1) and (2) can be solved numerically. Unfortunately, the complexity of these equations means that orbit perturbation calculations can be computationally expensive. To overcome this, we can make some simplifying assumptions. For example, the nonlinearity of thermal emission on the surface can be dealt with by assuming that the temperature throughout the body is close to an average value T_0 (i.e., $T = T_0 + \Delta T$ with $\delta = (\Delta T/T_0) \ll 1$. If T_0 is constant, equations (1) and (2) may be rewritten for the δ variable, while the fourth-order term in the boundary condition (equation (2)) may be simplified as $T^4 \approx T_0^4 (1 + 4\delta + \ldots)$.

At this point, we find it useful to scale size and time so that minimum parameters are retained in the mathematical formulation of the problem. For example, dimensional analysis shows that, for a given Fourier term with frequency ν in the decomposition of the insolation function $\mathcal{E}$, the problem involves two fundamental parameters: (1) the penetration depth of the thermal wave $\ell_\nu = \sqrt{K/\rho C\nu}$, and (2) the thermal parameter $\Theta_\nu = \sqrt{K\rho C\nu}/(\varepsilon\sigma T_\star^3)$ (here $T_\star$ is the sub-

solar temperature defined by $\varepsilon\sigma T_\star^4 = \alpha\mathcal{E}_\star$ with $\mathcal{E}_\star$ being the solar radiation flux at the distance of the body). The thermal parameter Θ_ν is a measure of the relaxation between the absorption and reemission at frequency ν. Thus, as Θ_ν decreases, the difference between the absorption and reemission decreases as well.

Assuming a spherical body rotating about an arbitrary axis, the spectrum of the insolation function consists primarily of the "diurnal line" with rotation frequency ω (and its multiples) and the "seasonal line" with the mean-motion frequency n. Note that orbital eccentricity adds higher multiples of the mean-motion frequency, increasing algebraic complexity, while also weakening the assumption of the linearized approach (temperature changes cannot be represented as small variations around a constant average value). Fortunately, most applications of the Yarkovsky effect involve main belt bodies on low-eccentricity orbits. Assuming a small eccentricity, the solution of the amplitudes of the Fourier representation of δ as a function of the spatial coordinates can be worked out analytically.

Having solved the temperature T, or the linearized quantity δ, we can proceed to compute the recoil force (or torque) due to the thermal radiation (i.e., the Yarkovsky force). Assuming isotropic (Lambert) emission, the corresponding force per unit of mass is given by

$$\mathbf{f} = -\frac{2}{3}\frac{\varepsilon\sigma}{mc}\int_s dS(u,v)T^4\mathbf{n}_\perp \qquad (3)$$

where the integration is to be performed over the whole surface parameterized by a system of coordinates u and v (such as the longitude and latitude in the spherical case), m is the mass of the body, and c is the light velocity. The integral in equation (3) may be evaluated numerically, or we may again refer to linearization of the fourth power of the temperature as mentioned above and perform the integration analytically.

Adopting a local coordinate system with the z-axis aligned with the body's spin axis and the xy-axes in its equatorial plane, the linearized solutions suggest a useful classification of two variants of the Yarkovsky force: (1) The out-of-spin components of the Yarkovsky acceleration (f_x, f_y) depend primarily on the rotation frequency ω (with typically unimportant splitting $\omega \pm n$ due to the orbital motion; *Vokrouhlický,* 1999), while (2) the spin-aligned component of the Yarkovsky acceleration f_z depends only on the mean motion n. The former Yarkovsky-acceleration components are thus called "diurnal," while the latter is called "seasonal" (and they correspond to the qualitative concepts discussed in section 2). It should be noted that splitting the Yarkovsky effect into these two variants is an artifact of the linearized solution. In the more complete formulation, the effects are coupled.

Yarkovsky accelerations primarily change orbital semimajor axis a. Since the perturbation is usually small, we average the variation in a over one revolution. Assuming a spherical body with radius R, and neglecting eccentricity e, the averaged diurnal and seasonal perturbations on da/dt are

$$\left(\frac{da}{dt}\right)_{diurnal} = -\frac{8\alpha}{9}\frac{\Phi}{n}F_\omega(R',\Theta)\cos\gamma + \mathcal{O}(e) \qquad (4)$$

$$\left(\frac{da}{dt}\right)_{seasonal} = \frac{4\alpha}{9}\frac{\Phi}{n}F_n(R',\Theta)\sin^2\gamma + \mathcal{O}(e) \qquad (5)$$

The total da/dt rate is the superposition of the two variants. The albedo-factor α in equation (4) and equation (5) is close to that in equation (2) (*Vokrouhlický and Bottke,* 2001), $\Phi = \pi R^2\mathcal{E}_0/(mc)$ is the usual radiation pressure coefficient, and γ is obliquity of the spin axis. The function $F_\nu(R',\Theta)$ depends on the radius of the body R, scaled by the penetration depth ℓ_ν of the thermal wave ($R' = R/\ell_\nu$) and the thermal parameter Θ_ν, both corresponding to the frequency ν. For the diurnal effect, $\nu = \omega$, while for the seasonal effect, $\nu = n$. Note that apart from the different frequency, F is the same in equations (4) and (5). The explicit form of F function may be found in the literature (e.g., *Vokrouhlický*, 1998a, 1999). Here we restrict ourselves to mentioning its dependence on the thermal parameter

$$F_\nu(R',\Theta) = -\frac{\kappa_1(R')\Theta_\nu}{1 + 2\kappa_2(R')\Theta_\nu + \kappa_3(R')\Theta_\nu^2} \qquad (6)$$

with κ_1, κ_2, and κ_3 analytic functions of R'. The frequency-index of F reminds us that both the scaling factor ℓ_ν of R and the thermal parameter Θ_ν depend on a given frequency. This parameter is the principle difference between the diurnal and seasonal Yarkovsky effects.

The da/dt rates listed above give us a basic understanding of how the Yarkovsky perturbations depend on a number of parameters:

1. *Obliquity and rotation dependence:* Since the F functions are always negative (i.e., thermal reemission lags behind the absorption) the seasonal Yarkovsky effect always produce a net decrease in a. The seasonal effect is maximum at 90° obliquity and nil at 0° (or 180°) obliquity. On the other hand, the diurnal effect may lead to both a net increase in a (for $\gamma < 90°$) or a net decrease in a (for $\gamma > 90°$). The effect is maximum at 0° (or 180°) obliquity and nil for 90° obliquity. The diurnal Yarkovsky effect becomes negligible in the limit of infinitely fast rotation, since surface temperature variations are smeared along lines of constant latitude, and zero rotation.

2. *Size dependence:* The Yarkovsky effect vanishes for both very small and very large objects. For large objects, $(da/dt) \approx \Theta/R'$, where the $\approx 1/R$ dependence arises from the body's cross-section vs. its mass. For small objects, $(da/dt) \approx R'^2/\Theta$. The maximum drift in a occurs when $R' \approx 1$ (i.e., when the body's size is comparable to the penetration depth of the corresponding thermal wave).

3. *Surface-conductivity dependence:* Surface conductivity K is the major thermal material parameter that influences the strength of the Yarkovsky effect. It ranges from very low values for highly porous or regolith-like surfaces

(≈ 0.001 W m^{-1} K^{-1}), to moderate values for bare rocks such as ordinary chondrites or icy objects (≈1 W m^{-1} K^{-1}), up to high values for iron-rich objects like iron meteorites (≈ 40 W m^{-1} K^{-1}). Variations of K modify ℓ_γ and Θ_γ. At low conductivities, we expect that Θ will be small and R' large, since the penetration depth of the corresponding thermal wave decays to zero. Thus, (da/dt) ≈ Θ and the Yarkovsky effect disappears. For high conductivities, the thermal parameter diverges and the scaled radius of the body tends to zero, since the penetration depth of the corresponding thermal wave diverges. Thus, (da/dt) ≈ R'^{2}/Θ, yielding very fast decay of the Yarkovsky effect as the body is driven toward thermal equilibrium. Maximum da/dt rates occur when both R' ≈ 1 and Θ ≈ 1.

4. *Solar-distance dependence:* The Yarkovsky effect decreases with increasing distance to the Sun. In case of the diurnal effect, objects are usually in the high-Θ and high-R' regime, so that (da/dt) ≈ Φ/(nΘ). From the functional dependence of Φ, n, and Θ on a, we derive (da/dt) ≈ a^{-2} (e.g., *Radzievskii,* 1952; *Peterson,* 1976). Thus, the diurnal effect dwindles very fast with increasing distance from the Sun, with very slowly rotating bodies a possible exception. A comparable analysis for the seasonal effect is more involved since F_n cannot be approximated as ≈1/Θ. An example of this would be 0.1–1-km icy bodies in the Kuiper Belt, whose seasonal da/dt drift rates become much shallower as a function of distance from the Sun. This surprising result occurs because the penetration depth of the seasonal thermal wave ℓ_n increases to ~0.1 km.

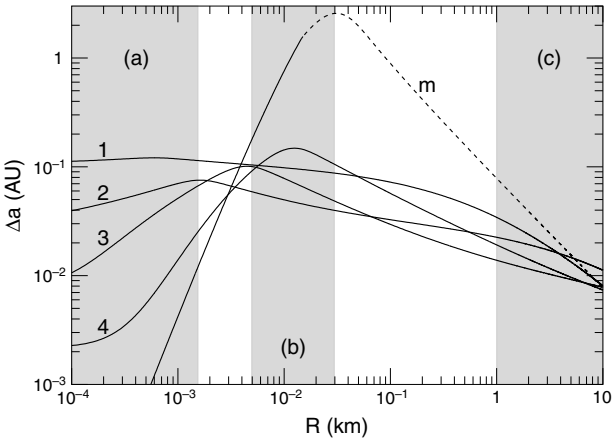

Fig. 2. Mean change of the semimajor axis Δa (in AU) of inner-main-belt asteroids over their collisional lifetimes (see text) vs. their radius R (in kilometers). Both components (diurnal and seasonal) of the Yarkovsky effect are included. Five different values of the surface conductivity K are considered: (1) K = 0.002 W m^{-1} K^{-1}; (2) K = 0.02 W m^{-1} K^{-1}; (3) K = 0.2 W m^{-1} K^{-1}; (4) K = 2 W m^{-1} K^{-1}; and (5) K = 40 W m^{-1} K^{-1} (curve m, for metal-rich bodies). The low-K cases are dominated by the diurnal effect, while for high-K cases the seasonal effect is more important. The dashed strips correspond to three astronomically important classes of bodies: **(a)** preatmospheric meteorite parent bodies (R = 0.1–1.5 m); **(b)** Tunguska-like small NEAs (R = 5–30 m); and **(c)** the largest existing NEAs or the smallest observed family members (R = 1–10 km). Note that Δa depends sensitively on the selected value of K in the **(a)** and **(b)** size ranges, but much less so in range **(c)**.

4. SEMIMAJOR AXIS MOBILITY OF ASTEROID FRAGMENTS

Using the above equations, *Farinella and Vokrouhlický* (1999) computed the average semimajor axis displacement (Δa) of main-belt meteoroids and asteroids caused by the Yarkovsky effect before undergoing a catastrophic disruption (Fig. 2). The collision lifetime of the objects, τ_{disr}, was assumed to be $\tau_{disr} \simeq 16.8 \sqrt{R}$ m.y., with R being the body's radius in meters. The objects were started with random obliquity orientations (γ), but were also assumed to go through spin axis reorientation events via nondisruptive impacts. The characteristic timescale of these events was assumed to be $\tau_{rot} \simeq 15.0 \sqrt{R}$ m.y. (*Farinella et al.,* 1998). Rotation rates were assumed to be correlated with size through the relation P = 5 R where P is the rotation period in seconds and R the radius in meters. Since surface conductivity K for asteroids is unknown, several different values of K were selected.

We point out several interesting results from Fig. 2. (1) Except for the high-strength iron objects, the maximum expected drift distance from these mean values was on the order of 0.1 AU. (2) Δa becomes smaller for large bodies (down to 0.01 AU at R ≃ 5–10 km). The dependence on surface conductivity, however, becomes much less important. (3) High-conductivity objects (curve 4 in Fig. 2) have maximum mobility for R ≈ 10 m, primarily because of the seasonal Yarkovsky effect (*Rubincam,* 1998; *Farinella et al.,* 1998). (4) Characteristic Δa values of ≈ 0.1 AU for smaller asteroids and ≈ 0.01 AU for kilometer-sized asteroids have important dynamical consequences. For instance, 0.1–0.2 AU is a typical distance that a main-belt meteoroid might have to travel to reach a powerful main belt resonance. Similarly, 0.01–0.02 AU is a typical semimajor axis span of asteroid families, whose observed components are dominated by multikilometer bodies. More details about these applications will be given below.

5. APPLICATIONS OF THE YARKOVSKY EFFECT

5.1. Delivery of Meteoroids from the Main Belt to Earth

The original motivation behind the Yarkovsky effect was related to the transport of small bodies from the main belt to Earth (*Öpik,* 1951; *Radzievskii,* 1952; *Peterson,* 1976). At the time of these papers, it was unclear whether collisional and dynamical processes were efficient enough to explain the overall flux of meteorites reaching Earth, let alone the CRE ages of stony meteorites (e.g., *Wetherill,* 1974). For this reason, these researchers hypothesized that the Yarkovsky effect might deliver meteoroids from the main belt to Earth via a slow decay of their semimajor axes.

The timescales involved with this scenario, however, were too long to be considered practical, particularly when reasonable meteoroid rotation rates were used.

The apparent solution to this meteoroid delivery problem was found in the pioneering works of Williams (see *Wetherill,* 1979) and *Wisdom* (1983), who showed that powerful mean-motion and secular resonances in the inner main belt could potentially move main-belt bodies onto Earth-crossing orbits within relatively short timescales (~1 m.y.). Thus, a plausible scenario for explaining the CRE ages of stony meteorites became the following: (1) collisions in the main belt inject fragments into resonances, (2) the fragments evolve onto Earth-crossing orbits via resonant motion, (3) close encounters remove the objects from resonance, and (4) the objects wander the inner solar system for 10–100 m.y. before striking a terrestrial planet, being ejected from the inner solar system by Jupiter, or experiencing a collisional disruption event. Since Monte Carlo code results verified the main components of this model (e.g., *Wetherill,* 1985), the Yarkovsky effect came to be viewed as an unneeded complication and was summarily dropped from consideration by most dynamicists.

Problems with this scenario began to present themselves in the 1990s as fast workstations and efficient numerical integrations codes began to overtake Monte Carlo codes as the dominant means of tracking the evolution of small bodies in the solar system. The major blows came from *Farinella et al.* (1994), who showed that many resonant objects strike the Sun, and *Gladman et al.* (1997), who showed that bodies escaping the main belt via the 3:1 mean-motion resonance with Jupiter or the ν_6 secular resonance only had a mean dynamical lifetime of ~2 m.y. As described in section 1, these lifetimes are largely discordant with the CRE ages of stony and iron meteorites (e.g., *Morbidelli and Gladman,* 1998).

Farinella et al. (1998), however, recognized that the explanation to the CRE problem might be the Yarkovsky effect, since it could slowly deliver material to powerful resonances inside the main belt. [Note that this scenario had been previously suggested by both *Peterson* (1976) and *Afonso et al.* (1995). Unfortunately, the implications of their work were overlooked, primarily because (1) the CRE age of stony meteorites were consistent with dynamical lifetimes derived from Monte Carlo codes (i.e., *Wetherill,* 1985) and (2) results from more accurate numerical integration codes were not yet in hand (e.g., *Dones et al.,* 1999).] As these bodies drifted toward an escape hatch (typically 0.05–0.15 AU), they would be hit by cosmic rays, which would push their CRE ages into the appropriate range. In addition, because iron meteorites have very different thermal conductivities than stones, their da/dt rates are slow enough to explain their long CRE ages (0.1–1.0 G.y.). Thus, the Yarkovsky effect provides a natural explanation for the paucity of short CRE ages among stony meteorites and the differences in the observed CRE ages of stony and iron meteorites.

The dynamical evolution of main-belt meteoroids can be surprisingly complex. As described in the previous section, the drift rate for meter-sized stones in the main belt is $\pm$(0.01–0.001) AU m.y.$^{-1}$, depending on their spin axis orientation, spin rate, and thermal properties. Numerical integration work by *Bottke et al.* (2000a) and *Brož et al.* (2002) have shown that these da/dt drift rates are fast enough to allow meteoroids to "jump over" most weak resonances, effectively accelerating their drift rate. Most meteoroids will spiral inward or outward until they become trapped in a powerful resonance too chaotic to jump (e.g., the 3:1 or ν_6 resonance). En route, some may become temporarily trapped in weak mean-motion or secular resonances, allowing their e and i values to undergo secular changes while a remains fixed. If a meteoroid's e oscillations reach a high enough amplitude, it may escape the main belt via a close encounter with Mars. Additional complications come from nondisruptive collisions, since they can modify the meteoroid's spin axis orientation and spin rate. Thus, objects drifting via the Yarkovsky effect may well reverse course and speed several times before reaching a powerful resonance.

Although tracking the dynamical evolution of individual meteoroids via the Yarkovsky effect requires careful work, the evolution of large "swarms" of fragments, released by catastrophic break-up events or impacts on large asteroids in the main belt, can be modeled statistically. To this end, the most successful effort so far to combine dynamics, collisions, and the Yarkovsky effect into a meteoroid evolution code has been the work of *Vokrouhlický and Farinella* (2000). In their model, they started with a size distribution of small bodies ejected from a chosen parent asteroid, with each body having its own spin rate and spin axis orientation. Using simplified dynamics, they tracked these bodies across the inner main belt to the 3:1 or ν_6 resonance, assuming that their da/dt drift rates were not influenced by smaller resonances. Collisions were also included, with random impact events producing cascades of new fragments from the disruption of the existing bodies. When the objects reached the 3:1 or ν_6 resonance, Yarkovsky evolution was shut off and the bodies were delivered to Earth via statistical results taken from the numerical simulations of *Morbidelli and Gladman* (1998).

The combination of the two studied phenomena — Yarkovsky drift and collisional dynamics — was found to efficiently supply the 3:1 and ν_6 resonances with small asteroid fragments from nearly all locations in the inner and central main belt. Direct injections, considered in "pre-Yarkovsky" studies (e.g., *Farinella et al.,* 1993), only seem important when a source is close to a resonance. Moreover, the flux of objects to the resonances is, contrary to the direct-injection scenario, spread over hundreds of millions of years, as the collisional cascade creates fast-drifting fragments from larger, slower-drifting progenitors. For example, *Vokrouhlický and Farinella*'s (2000) results indicate that 50–80% of the mass of the initial population of bodies released in the Flora-region are transported to resonances (dominantly the ν_6 resonance) over 0.5 to 1 G.y.

Another important result from this model is that the distribution of accumulated CRE ages in the population of

fragments reaching Earth is in reasonable agreement with observations (e.g., *Marti and Graf,* 1992; *Welten et al.,* 1997). In general, the CRE age histograms are found to depend on the age of the last event capable of dominating the local Earth swarm. Relatively old events are likely to generate the background CRE age profiles (like in the case of L chondrites) peaked at 20–50 m.y. for stones and 200–500 m.y. for irons, while comparatively recent and large events may create discrete peaks in the CRE age distributions (such as the 7–8 m.y. prominent peak for the H chondrites). In the latter case, the bulk of the original fragment population may still reside in the main belt and will supply a significant flux of meteorites in the future. Figure 3 shows comparison of the simulated and observed CRE ages for different types of meteorites and different parent asteroids.

5.2. Escape of Kilometer-sized Asteroids from the Main Belt

Dynamical modeling suggests most Earth- and Mars-crossing asteroids ultimately come from the main belt (e.g., *Bottke et al.,* 2000b, 2002a). The cratering records of the terrestrial planets suggest this joint population, containing 5000–6000 D > 1 km asteroids of various taxonomic types, has been more or less in steady state for the last 3 G.y. (e.g., *Grieve and Shoemaker,* 1994). The primary sources of these bodies are the 3:1 mean-motion resonance with Jupiter, the ν_6 secular resonance, and numerous narrow mean-motion resonances produced by Mars or the combined effects of Jupiter and Saturn (*Wisdom,* 1983; *Morbidelli and Gladman,* 1998; *Migliorini et al.,* 1998; *Morbidelli and Nesvorný,* 1999). The viability of these sources have been checked using sophisticated numerical integration codes that track test asteroids evolving under the combined perturbations of the Sun and planets for ~100 m.y. (*Wisdom and Holman,* 1991; *Levison and Duncan,* 1994).

A possible problem with these simulations, however, is that they do not consider how the test asteroids reach their starting orbits. As described in the introduction, previous work has assumed that asteroids are thrown directly into resonances by main-belt collisions (e.g., *Farinella et al.,* 1993). The combined width of resonances in the inner and central main belt, however, is small enough that collisions alone may be unable to keep them filled with debris (*Farinella and Vokrouhlický,* 1999). Dynamical models suggest a shortage of resonant material could eventually lead to a discernible depletion of inner solar system asteroids (*Migliorini et al.,* 1998; *Michel et al.,* 2000). This problem would also be exacerbated by the fact that most potential parent bodies are located far from resonant escape hatches, and that the disruption of large bodies in the inner main belt should produce observable asteroid families.

For these reasons, *Farinella and Vokrouhlický* (1999) postulated that most main-belt resonances are restocked with D ≲ 20-km asteroids via the Yarkovsky effect. This potential solution could explain the spectral diversity of the inner solar system asteroid population (e.g., *Binzel et al.,* 2001) as well as well as the slope of its size-frequency distribution, which is shallower [N(>D) ∝ $D^{-1.75}$ (*Bottke et al.,* 2000a)] than one might expect if fresh ejecta were being launched directly into resonances [N(>D) ∝ D^{-3} (*Tanga et al.,* 1999)] but, at the same time, only slightly steeper than the population of main-belt asteroids in this size range [N(>D) ∝ D^{-1} (*Durda et al.,* 1998; *Davis et al.,* 2002)].

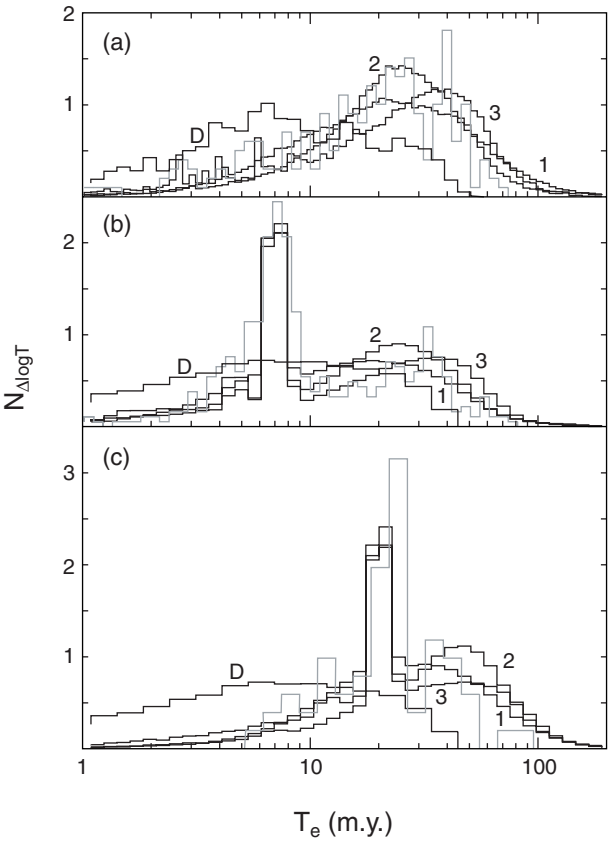

Fig. 3. Comparison of the modeled and observed CRE-age distributions for three different meteorite types (data — gray histograms). We show results of the direct-injection scenario with no Yarkovsky mobility (D histogram) and the model including Yarkovsky mobility of the meteoroids and their precursors (bold full-line histograms). Histograms 1, 2, and 3 refer to thermal conductivity values of 0.0015, 0.1, and 1 W m^{-1} K^{-1} respectively. **(a)** Assumes ejecta from asteroid Flora whose computed CRE ages are compared with the observed distribution for 240 L chondrites. **(b)** Assumes ejecta from asteroid (6) Hebe and the comparison with 444 CRE ages of H chondrites. **(c)** Assumes ejecta from asteroid (4) Vesta, compared to the CRE age data for 64 HED (howardite-eucrite-diogenite) meteorites. In all cases, the intermediate K value appears to provide the best match to the data. Note that the direct-injection scenario would always predict many more short CRE ages than are observed, as well as a shortage of ages between 20 and 50 m.y., which is not observed.

To investigate this scenario, *Bottke et al.* (2002b) numerically integrated hundreds of test asteroids in the inner (2.1–2.48 AU) and central (2.52–2.8 AU) main belt with and without the Yarkovsky effect. The orbits of the test asteroids were chosen to be a representative sample of the observed population residing near (but not on) Mars-crossing

orbits (perihelion q ≥ 1.8 AU). Where possible, these tests duplicated the initial conditions investigated by *Migliorini et al.* (1998) and *Morbidelli and Nesvorný* (1999). All these test asteroids were tracked for at least 100 m.y. using a numerical integration code modified to accommodate Yarkovsky thermal forces (*Levison and Duncan,* 1994; *Bottke et al.,* 2000b; *Brož et al.,* 2002). A wide range of asteroid diameters (0.2 km, 0.4 km, 2 km, 4 km, 10 km) were used. Objects in the inner and central main belt were given S-type and C-type albedos respectively. Thermal conductivities were chosen to be consistent with values expected from regolith-covered asteroids. Random spin axis orientations and size-dependent spin rates were also used (e.g., *Bottke et al.,* 2000a). All these tests were compared to a control case where the Yarkovsky effect was turned off.

Bottke et al. (2002b) found that Yarkovsky-driven objects with D > 2 km reached Mars-crossing orbits at the same rate as the control case, despite the fact that the dynamical evolution of individual bodies in each set could be quite different (Fig. 4). For example, D = 10-km objects, with slow drift rates (e.g., Fig. 2), followed dynamical paths that were more or less analogous to the results of *Migliorini et al.* (1998) and *Morbidelli and Nesvorný* (1999). In this case, secular increases in e were caused predominantly by the bodies interacting with overlapping mean-motion resonances near the main belt periphery. On the other hand, resonant trapping does not appear to be the dominant behavior of D < 2-km objects; their faster drift rates allow many them to jump across many numerous weak resonances as they drift into the Mars-crossing region. In general, small inner-main-belt asteroids do not stop until they reach the wide and powerful 3:1 mean-motion resonance with Jupiter, the ν_6 secular resonance, or the Mars-crossing region itself. *Bottke et al.* (2002b) concluded from these results that the Yarkovsky effect was more efficient at driving subkilometer bodies out of the main belt than multikilometer bodies. The major source regions for subkilometer asteroids in the inner solar system should be powerful resonances like the 3:1 or ν_6 resonances, while an important source for multikilometer bodies would be the numerous tiny resonances scattered throughout the main belt (and possibly secular resonances intersecting asteroid families; see next section). *Bottke et al.* (2002a) estimate that the combined flux of kilometer-sized bodies from these sources is ~220 per million years. This rate is high enough to suggest the Yarkovsky effect, rather than collisional injection, is the dominant mechanism pushing material into resonances. It also suggests that some main-belt asteroid sources may produce more large or small objects than other sources. A considerable amount of work will be needed to fully appreciate all the ramifications of this new asteroid delivery scenario.

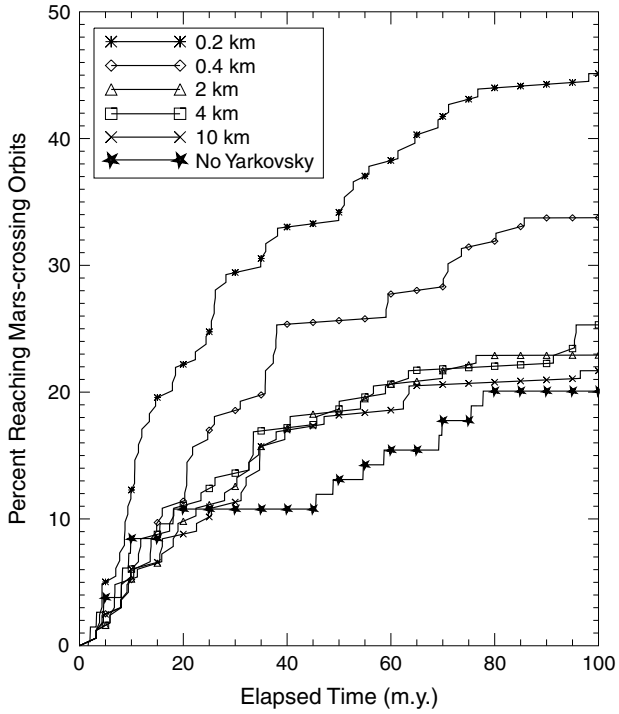

Fig. 4. Evolution of nearly-Mars-crossing bodies under the influence of Yarkovsky thermal forces. The plot shows the fraction of test asteroids, started with perihelion q ≥ 1.8 AU, reaching Mars-crossing orbits after 100 m.y. of integration. The initial conditions of the test asteroids nearly duplicated the initial conditions of *Morbidelli and Nesvorný* (1999). The bottom curve shows the *Morbidelli and Nesvorný* (1999) results. Results indicate that roughly the same fraction of D > 2-km bodies reach Mars-crossing orbits after 100 m.y., with or without Yarkovsky. Asteroids with D < 2 km, however, are much more efficient at escaping the main belt.

5.3. Dynamical Spreading of Asteroid Families

Asteroid families are remnants of large-scale catastrophic collisions. They are usually identified by their orbital elements, which tend to be clustered at similar values (e.g., *Bendjoya et al.,* 2002). By studying asteroid families, we hope to learn more about asteroid impacts, the primary geologic process occurring on asteroids today. Despite extensive work on this topic, however, there are still many issues related to asteroid families that we do not yet understand. We list a few below.

1. *Velocity distributions.* If one assumes that the semimajor axis distribution of family members has been constant since the formation event, it is possible to deduce the original ejection velocities of the fragments (*Zappalà et al.,* 1996). The inferred velocity distributions from this technique, on order of several 100 m s^{-1}, are inconsistent with ejection velocities derived by other means [i.e., laboratory impact experiments and numerical hydrocodes suggest multikilometer bodies typically have ejection velocities on the order of 100 m s^{-1} (*Benz and Asphaug,* 1999)].

2. *Orbital distributions.* Many prominent asteroid families have asymmetric (a, e, i) distribution. For example, Fig. 5 shows the distribution of the Koronis family in proper (a, e). Note that family members with small proper a are far less dispersed in proper e than those with large proper a, while both ends of the family are truncated by powerful

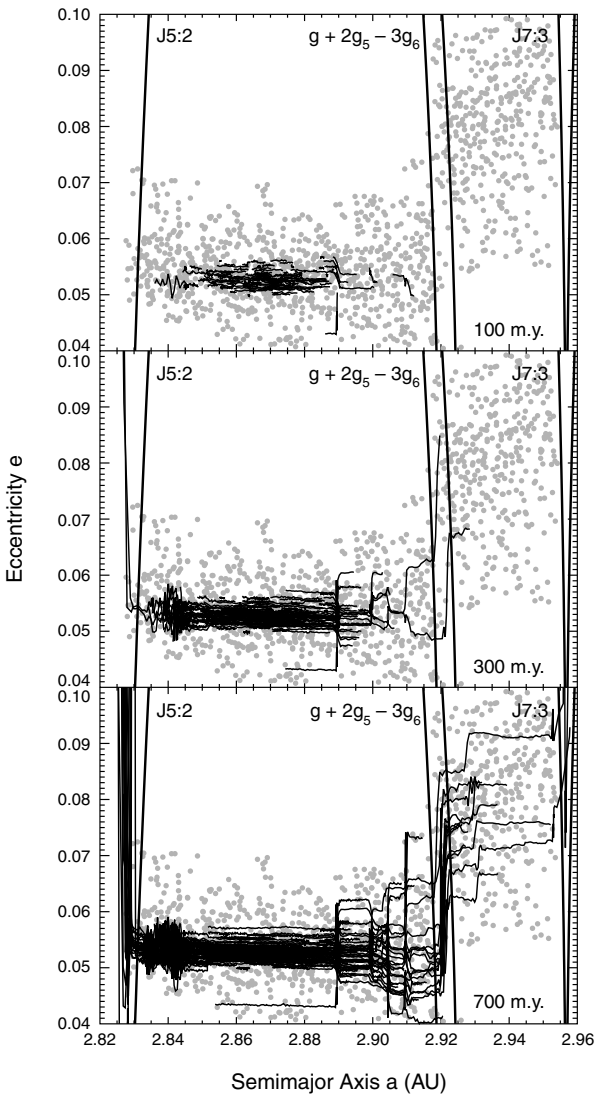

Fig. 5. Evolution of 210 simulated Koronis family members via the Yarkovsky effect (*Bottke et al.*, 2001). The test family members (black lines) were started within ~60 m s^{-1} of (158) Koronis (proper elements a = 2.87 AU, e = 0.045, sin i = 0.038) and were integrated for ~700 m.y., short compared with the estimated age of the family (~2.5 G.y.) but enough to determine evolution trends. The orbital tracks were averaged over a running 10-m.y. window in order to compare them with the proper (a, e) of the Koronis family members (gray dots). Snapshots of the integration tracks, shown at 100 m.y., 300 m.y., and 700 m.y., indicate these bodies interact with several resonances between 2.89 and 2.93 AU, with the secular $g + 2g_5 - 3g_6$ resonance at 2.92 AU being most prominent. These jumps allow the simulated family members to reach the (a, e) positions of many real family members. Fast-drifting bodies are seen to escape the main belt via the 5:2 and 7:3 mean-motion resonances with Jupiter.

mean-motion resonances with Jupiter (i.e., 5:2 on the left, 7:3 on the right). Surprisingly, no family members appear to have crossed either resonance, even though the 5:2 and 7:3 resonances are relatively narrow when compared to the span of the family.

3. *Family members on short-lived orbits.* Some multikilometer members of asteroid families are "on the brink" of entering a resonance [e.g., Koronis family members (*Milani and Farinella,* 1995; *Knežević et al.,* 1997; *Vokrouhlický et al.,* 2001)], are already inside a powerful resonances [e.g., Eos family members (*Zappalà et al.,* 2000)], or are part of the relatively short-lived NEO population [V-type asteroids, which presumably are part of the Vesta family (*Migliorini et al.,* 1997)]. Since most large families are thought to be 1 G.y. old or more (*Marzari et al.,* 1995), it is hard to understand how these family members attained these orbits. Using the classical model, one might assume that secondary fragmentation moved these objects onto their current orbits, but the large size of some of the objects (D > 10 km) makes this scenario improbable.

One way to resolve these issues is to assume that family members, since their formation, have migrated via the Yarkovsky effect. As shown in Fig. 2, an ensemble of D = 5-km asteroids will move inward and outward at mean drift rates of $|da/dt| \sim 2 \times 10^{-5}$ AU $m.y.^{-1}$, while larger asteroids drift more slowly (e.g., D ~20-km asteroids drift at $|da/dt| \sim 6 \times 10^{-6}$ AU $m.y.^{-1}$). Since collisional models suggest that many asteroid families are hundreds of millions of years to billions of years old (*Marzari et al.,* 1995, 1999), the potential drift distances of these objects are large enough to explain the observed dispersions of many asteroid families. Moreover, since Yarkovsky drift is size-dependent, the family members would eventually take on the appearance that they were launched using a size-dependent velocity distribution.

Thus, according to this scenario, the observed asteroid families were created through a multistep process. (1) A large asteroid undergoes a catastrophic disruption and ejects fragments at velocities consistent with those found in laboratory experiments and hydrocode simulations. (2) D < 20-km fragments, whose initial velocity dispersion is smaller than those currently observed among asteroid families, start drifting in semimajor axis under the Yarkovsky effect. D > 20-km fragments, which are less susceptible to the Yarkovsky effect, mainly move in semimajor axis via less efficient processes like collisions and/or close encounters with asteroids like Ceres, Pallas, or Vesta (*Carruba et al.,* 2000; *Nesvorný et al.,* 2002). (3) D < 20-km fragments, whose drift rate is a function of each object's size, spin state, and thermal properties, jump over or become trapped in chaotic mean-motion and secular resonances that change their eccentricity and/or inclination. In some cases, these orbital changes are significant enough that the objects can no longer be easily recognized as family members. (4) Family members that drift far enough may fall into mean-motion or secular resonances capable of pushing them onto planet-crossing orbits. From here, they become members of the Mars-crossing and/or NEO populations.

To check this idea, *Bottke et al.* (2001) tracked the evolution of test asteroids started close to the center of the Koronis family using the symplectic integration code SWIFT-RMVS3, which was modified to accommodate Yarkovsky thermal forces (*Levison and Duncan,* 1994; *Bottke et al.,* 2000b; *Brož et al.,* 2002). Figure 5 shows Yarkovsky forces

driving multikilometer asteroids through numerous secular resonances where resonant jumping/trapping events produce noticeable changes in proper e, particularly on the right side of the plot. The most significant jumps are caused by the secular resonance $g + 2g_5 - 3g_6$ at 2.92 AU, which increases e but does not change i. Eventually, objects drifting far enough become trapped in the powerful 5:2 or 7:3 mean-motion resonances, where they are pushed onto planet-crossing orbits and are lost from the main belt.

Overall, these integration results reproduce the (a, e, i) distribution of the Koronis family while also explaining the paucity of family members on the left/right sides of the 5:2 and 7:3 resonances and the short-lived nature of some Koronis family members. The success of this model, together with the previous section's results, make a strong case that the Yarkovsky effect, working in concert with resonances, is the primary mechanism by which D ≤ 20-km asteroids escape the main belt and reach the inner solar system.

5.4. Radiative Spinup/Spindown of Asteroids (YORP Effect)

Besides changing the orbit, Yarkovsky forces can also produce torques that affect the spin rate and spin axis orientation of asteroids and meteoroids. This "sunlight alters spin" mechanism was coined by *Rubincam* (2000) as the Yarkovsky-O'Keefe-Radzievskii-Paddack effect, or YORP for short (*Radzievskii,* 1954; *Paddack,* 1969, 1973; *Paddack and Rhee,* 1975; *O'Keefe,* 1976). YORP comes from two sources: reflection and reemission. *Rubincam* (2000) illustrated its workings using a rotating spherical asteroid with two wedges attached to the equator (Fig. 6). For a Lambertian radiator, the reaction force from photons departing from any given element of area on the sphere will be normal to the surface, such that no torque is produced. Energy reradiated from the wedges, however, can produce a torque because the wedge faces are not coplanar. For the sense of rotation shown in Fig. 6, the wedge-produced YORP torque spins the object up. If the body happened to spin in the opposite sense, the YORP torques would slow it down. Thus, an object must have some "windmill" asymmetry for YORP to work (i.e., it would have no effect on rotating triaxial ellipsoids).

YORP torques can also modify asteroid obliquities, which leads to the concept of the YORP cycle. For the geometry shown in Fig. 6, a fast-spinning asteroid would gradually increase its obliquity as well. When the obliquity becomes large enough, the axial torque changes sign and the object begins to spin down. This can be seen by imagining that the Sun shines down on the object from its north pole rather than the equator; the wedges must spin it the other way. Hence YORP may spin objects up for a while, but when the obliquity becomes large, they slow down and then perhaps tumble until they reestablish principal axis rotation, with the spin axis presumably pointing in a random direction. Then the cycle begins all over again, such that small solid objects probably avoid the "rotational bursting" envisioned by Radzievskii, Paddack, and O'Keefe (i.e., spinning a solid object so fast that it disrupts). Collisions large enough to modify an asteroid's spin axis orientation may also short-circuit a YORP cycle, potentially putting the object into an entirely different rotation state. Thus, YORP is most likely to be important in regimes where the YORP cycle is faster than the spin axis reorientation timescale via collisions (*Rubincam*, 2000; *Vokrouhlický and Čapek,* 2002).

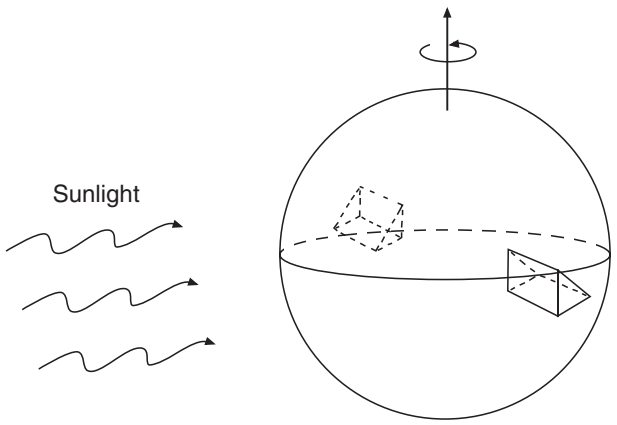

Fig. 6. Spinup of an asymmetrical asteroid. The asteroid is modeled as a sphere with two wedges attached to its equator. The asteroid is considered a blackbody, so it absorbs all sunlight falling upon it and then reemits the energy in the infrared as thermal radiation. Since the kicks produced by photons leaving the wedges are in different directions, a net torque is produced that causes the asteroid to spin up.

Rubincam (2000) found that YORP is strongly dependent on an asteroid's shape, size, distance from the Sun, and orientation. For example, assuming the Sun remains on the equator, asteroid (951) Gaspra, with R = 6 km and a = 2.21 AU, would in 240 m.y. go from a rotation period P = 12 h to 6 h (and vice versa). We call this value the YORP timescale. If we gave (243) Ida the same R and a values as Gaspra, it would have a YORP timescale half as big, while a body with Phobos' shape would have a YORP timescale of several billion years. Clearly, shapes make a big difference. The YORP timescale is also size-dependent (i.e., it goes as $\approx R^2$), such that smaller sizes spin up much more quickly. If Gaspra was only R = 0.5 km, its YORP timescale would be a few million years. Thus, YORP may be very influential for kilometer-sized and smaller asteroids. YORP is also more effective as you move closer to the Sun. Moving our R = 0.5 km Gaspra to 1 AU allows it to go from P = 12 h to rotational disruption speeds of ~2 h (and vice versa) in ~1 m.y. We caution, however, that YORP-induced obliquity torques may double or possibly triple the above timescales. Moreover, these rates also assume the YORP cycle continues without interruption via collisions, planetary close encounters, etc., and that asteroid thermal properties do not significantly change with size. These real-life complications will be modeled in the future.

If the aforementioned YORP timescales are reasonable values for small asteroids, it is plausible that YORP may

spin small gravitational aggregates up so fast that they are forced to "morph" into a new shape and/or undergo mass shedding. Since symmetrical shapes increase the YORP timescale, these shape changes may eventually strand some objects close to the rotational breakup limit. If rotational disruption is common, we hypothesize that YORP may supersede tidal disruption and collisions as the primary means by which binary asteroids are produced.

At this point, we can begin to explore the possible connection between asteroid spin rates and the YORP effect. Observations show that D > 125-km asteroids have rotation rates that follow a Maxwellian-frequency distribution, while 50 < D < 125-km asteroids show a small excess of fast rotators relative to a Maxwellian and D < 50-km asteroids show a clear excess of very fast and slow rotators (*Binzel et al.,* 1989). More recent observations indicate that D < 10-km asteroids have even more pronounced extrema (*Pravec and Harris,* 2000; *Pravec et al.,* 2002). These results suggest that one or more mechanisms are depopulating the center of the spin rate distribution in favor of the extremes, and that these mechanisms may be size-dependent.

The possible mechanisms capable of performing these spin modifications are (1) collisions; (2) tidal spinup/spindown via a close encounter with a planet; (3) tidal evolution between binary asteroids, where spin angular momentum is exchanged for orbital angular momentum (with possible escape); and (4) YORP. The limitations of (1)–(3) are described in *Pravec et al.* (2002) and will not be reviewed here. The advantage of YORP over these other mechanisms is that it can naturally produce both slow and fast rotation rates for small asteroids over relatively short timescales, and that it is a size-dependent effect, helping to explain why the spin rate distributions change with D. The disadvantage of YORP is that it does not appear to be capable of significantly modifying the spin rates of large asteroids by itself. A unified model, which includes these processes and YORP, however, might do a reasonable job at explaining the spin rates of large asteroids like (253) Mathilde. The solution is left to future work.

At the time of this writing, we consider YORP studies to be in their infancy. For example, *Vokrouhlický and Čapek* (2002) recently pointed out that the YORP-evolving rotation state may become temporarily locked in one of the resonances between the precession rate and the proper or forced frequencies of the long-term orbital-plane evolution. These effects may temporarily halt, reverse, or accelerate the YORP influence on the obliquity. Future work on the YORP effect must also take into account thermal relaxation, non-principal-axis rotation, and more refined thermophysics (e.g., *Spitale and Greenberg,* 2001a,b).

6. FUTURE WORK

At the present time, the existence of the Yarkovsky effect is mostly based on inferences (e.g., CRE age distribution of meteorites, origin of large NEAs, and size-dependent dispersion of the asteroid families). To conclusively prove the existence of the Yarkovsky effect, however, it would be useful to directly detect its orbital perturbation on asteroids in a manner consistent with what was done for the LAGEOS artificial satellite (e.g., *Rubincam,* 1987). *Vokrouhlický and Milani* (2000) and *Vokrouhlický et al.* (2000) have suggested that the Yarkovsky perturbations can be computed directly from radar observations of small NEAs like (1566) Icarus, (6489) Golevka, or 1998 KY26 over a period of years. The advantages of radar include precise astrometry (by a factor of 100–1000× better than the usual optical astrometry), information on asteroid physical parameters like shape/surface properties, and its rotation state, all useful for Yarkovsky modeling efforts. At the time of this writing, the necessary plans — including possible preapparition optical observations — are underway. If the modeling work of *Vokrouhlický et al.* (2000) is correct, radar observations during the next close encounters of the most promising candidate asteroids may produce a discernable Yarkovsky "footprint."

The biggest challenge for future Yarkovsky modeling will be combining Yarkovsky accelerations with YORP, particularly since there is a complicated interaction between rotation, orbit precession rates, and spin axis precession rates. For many asteroids, particularly those kilometer-sized and larger, the spin and orbital precession rates are comparable, such that we can expect complicated beatlike phenomena to affect obliquity over relatively short timescales (*Skoglöv,* 1999). Moreover, coupling between the rates may allow the spin axis to be captured into a spin-orbit resonance. All these factors produce complicated feedbacks that (1) can modify asteroid drift rates and rotation rate changes and (2) are difficult to predict without extensive modeling. Since YORP is sensitive to the size, shape, material properties, and asteroid location, this effect will also vary from object to object. Thus, though we have hopefully demonstrated the usefulness of including Yarkovsky forces into the classical asteroid evolution model, there is still much work left to be done.

Acknowledgments. The authors wish to acknowledge helpful reviews by J. Spitale and S. Dermott and support from NASA's Planetary Geology and Geophysics Program. We dedicate this chapter to the memory of John A. O'Keefe and Paolo Farinella, both of whom championed the importance of the Yarkovsky effect during their illustrious and distinguished careers. D. P. Rubincam would like to thank Milton Schach for helping stimulate the thoughts that led to the theoretical development of the seasonal Yarkovsky effect.

REFERENCES

Afonso G. B., Gomes R. S., and Florczak M. A. (1995) Asteroid fragments in Earth-crossing orbits. *Planet. Space Sci., 43,* 787–795.

Benz W. and Asphaug E. (1999) Catastrophic disruptions revisited. *Icarus, 142,* 5–20.

Bendjoya Ph. and Zappalà V. (2002) Asteroid family identification. In *Asteroids III* (W. F. Bottke Jr. et al., eds.), this volume. Univ. of Arizona, Tucson.

Binzel R. P., Farinella P., Zappalà V., and Cellino A. (1989) Aster-

oid rotation rates — Distributions and statistics. In *Asteroids II* (R. P. Binzel et al., eds.), pp. 416–441. Univ. of Arizona, Tucson.

Binzel R. P., Harris A. W., Bus S. J., and Burbine T. H. (2001) Spectral properties of near-Earth objects: Palomar and IRTF results for 48 objects including spacecraft targets (9969) Braille and (10302) 1989 ML. *Icarus, 151,* 139–149.

Bottke W. F., Nolan M. C., Greenberg R., and Kolvoord R. A. (1994) Velocity distributions among colliding asteroids. *Icarus, 107,* 255–268.

Bottke W. F., Jedicke R., Morbidelli A., Petit J., and Gladman B. (2000a) Understanding the distribution of near-Earth asteroids. *Science, 288,* 2190–2194.

Bottke W. F., Rubincam D. P., and Burns J. A. (2000b) Dynamical evolution of main belt meteoroids: Numerical simulations incorporating planetary perturbations and Yarkovsky thermal forces. *Icarus, 145,* 301–331.

Bottke W. F., Vokrouhlický D., Brož M., Nesvorný D., and Morbidelli A. (2001) Dynamical spreading of asteroid families via the Yarkovsky effect. *Science, 294,* 1693–1696.

Bottke W. F. Jr., Morbidelli A., Jedicke R., Petit J.-M., Levison H. F., Michel P., and Metcalfe T. S. (2002a) Debiased orbital and absolute magnitude distribution of the near-Earth objects. *Icarus, 156,* 399–433.

Bottke W. F., Vokrouhlický D., Brož M., and Morbidelli A. (2002b) Yarkovsky-assisted escape of kilometer-sized asteroids from the main belt. *Icarus,* in press.

Brož M., Vokrouhlický D., and Farinella P. (2002) Interaction of the Yarkovsky-driven orbits of meteoroids and their precursors with the weak resonances in the main belt. *Icarus,* in press.

Burns J. A., Lamy P. L., and Soter S. (1979) Radiation forces on small particles in the solar system. *Icarus, 40,* 1–48.

Caffee M. W., Reedy R. C., Goswami J. N., Hohenberg C. M., and Marti K. (1988) Irradiation records in meteorites. In *Meteorites and the Early Solar System* (J. F. Kerridge and M. S. Matthews, eds.), pp. 205–245. Univ. of Arizona, Tucson.

Carruba V., Burns J. A., Bottke W. F., and Morbidelli A. (2000) Asteroid mobility due to encounters with Ceres, Vesta, Pallas: Monte Carlo codes versus direct numerical integrations. *Bull. Am. Astron. Soc., 32,* 1406.

Cellino A., Michel P., Tanga P., Zappalà V., Paolicchi P., and Dell'Oro A. (1999) The velocity-size relationship for members of asteroid families and implications for the physics of catastrophic collisions. *Icarus, 141,* 79–95.

Davis D. R., Weidenschilling S. J., Farinella P., Paolicchi P., and Binzel R. P. (1989) Asteroid collisional history — Effects on sizes and spins. In *Asteroids II* (R. P. Binzel et al., eds.), pp. 805–826. Univ. of Arizona, Tucson.

Davis D. R., Durda D. D., Marzari F., Campo Bagatin A., and Gil-Hutton R. (2002) Collisional evolution of small body populations. In *Asteroids III* (W. F. Bottke Jr. et al., eds.), this volume. Univ. of Arizona, Tucson.

Dermott S., Durda D. D., Grogan K., and Kehoe T. J. (2002) Asteroidal dust. In *Asteroids III* (W. F. Bottke Jr. et al., eds.), this volume. Univ. of Arizona, Tucson.

Dohnanyi J. S. (1978) Particle dynamics. In *Cosmic Dust* (J. A. M. McDonnell, ed.), pp. 527–605. Wiley-Interscience, New York.

Dones L., Gladman B., Melosh H. J., Tonks W. B., Levison H. F., and Duncan M. (1999) Dynamical lifetimes and final fates of small bodies: Orbit integrations vs Öpik calculations. *Icarus, 142,* 509–524.

Farinella P. and Vokrouhlický D. (1999) Semimajor axis mobility of asteroidal fragments. *Science, 283,* 1507–1510.

Farinella P., Gonczi R., Froeschlé Cl., and Froeschlé Ch. (1993) The injection of asteroid fragments into resonances. *Icarus, 101,* 174–187.

Farinella P., Froeschlé C., Froeschlé C., Gonczi R., Hahn G., Morbidelli A., and Valsecchi G. B. (1994) Asteroids falling onto the Sun. *Nature, 371,* 315–316.

Farinella P., Vokrouhlický D., and Hartmann W. K. (1998) Meteorite delivery via Yarkovsky orbital drift. *Icarus, 132,* 378–387.

Gladman B. J., Migliorini F., Morbidelli A., Zappalà V., Michel P., Cellino A., Froeschlé C., Levison H. F., Bailey M., and Duncan M. (1997) Dynamical lifetimes of objects injected into asteroid belt resonances. *Science, 277,* 197–201.

Grieve R. A. F. and Shoemaker E. M. (1994) The record of past impacts on Earth. In *Hazards Due to Comets and Asteroids* (T. Gehrels and M. S. Matthews, eds.), pp. 417–462. Univ. of Arizona, Tucson.

Hartmann W. K., Farinella P., Vokrouhlický D., Weidenschilling S. J., Morbidelli A., Marzari F., Davis D. R., and Ryan E. (1999) Reviewing the Yarkovsky effect: New light on the delivery of stone and iron meteorites from the asteroid belt. *Meteoritics & Planet. Sci., 34,* 161–167.

Katasev L. A. and Kulikova N. V. (1980) Physical and mathematical modeling of the formation and evolution of meteor streams II. *Astr. Vestnik, 14,* 225–229.

Knežević Z., Milani A., and Farinella P. (1997) The dangerous border of the 5:2 mean motion resonance. *Planet. Space Sci., 45,* 1581–1585.

Levison H. F. and Duncan M. J. (1994) The long-term dynamical behavior of short-period comets. *Icarus, 108,* 18–36.

Marti K. and Graf T. (1992) Cosmic-ray exposure history of ordinary chondrites. *Annu. Rev. Earth Planet. Sci., 20,* 221–243.

Marzari F., Davis D., and Vanzani V. (1995) Collisional evolution of asteroid families. *Icarus, 113,* 168–187.

Marzari F., Farinella P., and Davis D. R. (1999) Origin, aging, and death of asteroid families. *Icarus, 142,* 63–77.

Michel P., Migliorini F., Morbidelli A., and Zappalà V. (2000) The population of Mars-crossers: Classification and dynamical evolution. *Icarus, 145,* 332–347.

Migliorini F., Morbidelli A., Zappalà V., Gladman B. J., Bailey M. E., and Cellino A. (1997) Vesta fragments from ν_6 and 3:1 resonances: Implications for V-type NEAs and HED meteorites. *Meteoritics & Planet. Sci., 32,* 903–916.

Migliorini F., Michel P., Morbidelli A., Nesvorný D., and Zappalà V. (1998) Origin of Earth-crossing asteroids: A quantitative simulation. *Science, 281,* 2022–2024.

Milani A. and Farinella P. (1995) An asteroid on the brink. *Icarus, 115,* 209–212.

Morbidelli A. and Gladman B. (1998) Orbital and temporal distributions of meteorites originating in the asteroid belt. *Meteoritics & Planet. Sci., 33,* 999–1016.

Morbidelli A. and Nesvorný D. (1999) Numerous weak resonances drive asteroids toward terrestrial planets orbits. *Icarus, 139,* 295–308.

Neiman V. B., Romanov E. M., and Chernov V. M. (1965) Ivan Osipovich Yarkovsky. *Earth and Universe, 4,* 63–64 (in Russian). (Translation into English by T. O. Laoghog available.)

Nesvorný D., Morbidelli A., Vokrouhlický D., Bottke W. F., and Brož M. (2002) The Flora family: A case of the dynamically dispersed collisional swarm? *Icarus,* in press.

O'Keefe J. A. (1976) *Tektites and Their Origin.* Elsevier, Amsterdam. 254 pp.

Olsson-Steel D. (1986) The origin of the sporadic meteoroid com-

ponent. *Mon. Not. R. Astron. Soc., 219,* 47–73.
Olsson-Steel D. (1987) The dispersal of the Geminid meteoroid stream by radiative effects. *Mon. Not. R. Astron. Soc., 226,* 1–17.
Öpik E. J. (1951) Collision probabilities with the planets and the distribution of interplanetary matter. *Proc. R. Irish Acad., 54A,* 165–199.
Öpik E. J. (1976) *Interplanetary Encounters: Close-Range Gravitational Interactions.* Elsevier, New York. 155 pp.
Paddack S. J. (1969) Rotational bursting of small celestial bodies: Effects of radiation pressure. *J. Geophys. Res., 74,* 4379–4381.
Paddack S. J. (1973) Rotational bursting of small particles. Ph.D. thesis, Catholic University,
Paddack S. J. and Rhee J. W. (1975) Rotational bursting of interplanetary dust particles. *Geophys. Res. Lett., 2,* 365–367.
Peterson C. (1976) A source mechanism for meteorites controlled by the Yarkovsky effect. *Icarus, 29,* 91–111.
Pisani E., Dell'Oro A., and Paolicchi P. (1999) Puzzling asteroid families. *Icarus, 142,* 78–88.
Pravec P. and Harris A. W. (2000) Fast and slow rotation of asteroids. *Icarus, 148,* 12–20.
Pravec P., Harris A. W., and Michalowski T. (2002) Spin rates of asteroids. In *Asteroids III* (W. F. Bottke Jr. et al., eds.), this volume. Univ. of Arizona, Tucson.
Radzievskii V. V. (1952) About the influence of the anisotropically reemited solar radiation on the orbits of asteroids and meteoroids. *Astron. Zh., 29,* 162–170.
Radzievskii V. V. (1954) A mechanism for the disintegration of asteroids and meteorites. *Dokl. Akad. Nauk SSSR, 97,* 49–52.
Rubincam D. P. (1987) LAGEOS orbit decay due to infrared radiation from earth. *J. Geophys. Res., 92,* 1287–1294.
Rubincam D. P. (1988) Yarkovsky thermal drag on LAGEOS. *J. Geophys. Res., 93,* 13805–13810.
Rubincam D. P. (1990) Drag on the LAGEOS satellite. *J. Geophys. Res., 95,* 4881–4886.
Rubincam D. P. (1995) Asteroid orbit evolution due to thermal drag. *J. Geophys. Res., 100,* 1585–1594.
Rubincam D. P. (1998) Yarkovsky thermal drag on small asteroids and Mars-Earth delivery. *J. Geophys. Res., 103,* 1725–1732.
Rubincam D. P. (2000) Radiative spin-up and spin-down of small asteroids. *Icarus, 148,* 2–11.
Skoglöv E. (1999) Spin vector evolution for inner solar system asteroids. *Planet. Space Sci., 47,* 11–22.
Slabinski V. J. (1977) Solar radiation torques on meteoroids: Complications for the Yarkovsky effect from spin axis precession. *Bull. Am. Astron. Soc., 9,* 438.
Spitale J. and Greenberg R. (2001) Numerical evaluation of the general Yarkovsky effect: Effects on semimajor axis. *Icarus, 149,* 222–234.
Spitale J. and Greenberg R. (2002) Numerical evaluation of the general Yarkovsky effect: Effects on eccentricity and longitude of periapse. *Icarus, 156,* 211–222.
Tanga P., Cellino A., Michel P., Zappalà V., Paolicchi P., and Dell'Oro A. (1999) On the size distribution of asteroid families: The role of geometry. *Icarus*, *141,* 65–78.
Vokrouhlický D. (1998a) Diurnal Yarkovsky effect as a source of mobility of meter-sized asteroidal fragments. I. Linear theory. *Astron. Astrophys., 335,* 1093–1100.
Vokrouhlický D. (1998b) Diurnal Yarkovsky effect as a source of mobility of meter-sized asteroidal fragments. II. Non-sphericity effects. *Astron. Astrophys., 338,* 353–363.
Vokrouhlický D. (1999) A complete linear model for the Yarkovsky thermal force on spherical asteroid fragments. *Astron. Astrophys., 344,* 362–366.
Vokrouhlický D. (2001) Yarkovsky effect: Many-fingered phenomenon in the solar system dynamics. In *The Restless Universe: Applications of Gravitational N-Body Dynamics to Planetary, Stellar and Galactic Systems* (B. A. Steves and A. J. Maciejewski, eds.), pp. 53–78. Institute of Physics, Bristol.
Vokrouhlický D. and Bottke W. F. (2001) The Yarkovsky thermal force on small asteroids and their fragments. Choosing the right albedo. *Astron. Astrophys., 371,* 350–353.
Vokrouhlický D. and Čapek D. (2002) YORP-induced long-term evolution of the spin state of small asteroids and meteoroids. I. Rubincam's approximation. *Icarus,* in press.
Vokrouhlický D. and Farinella P. (1998) The Yarkovsky seasonal effect on asteroidal fragments: A nonlinearized theory for the plane-parallel case. *Astron. J., 116,* 2032–2041.
Vokrouhlický D. and Farinella P. (1999) The Yarkovsky seasonal effect on asteroidal fragments: A nonlinearized theory for spherical bodies. *Astron. J., 118,* 3049–3060.
Vokrouhlický D. and Farinella P. (2000) Efficient delivery of meteorites to the Earth from a wide range of asteroid parent bodies. *Nature, 407,* 606–608.
Vokrouhlický D. and Milani A. (2000) Direct solar radiation pressure on the orbits of small near-Earth asteroids: Observable effects? *Astron. Astrophys., 362,* 746–755.
Vokrouhlický D., Milani A., and Chesley S. R. (2000) Yarkovsky effect on small near-Earth asteroids: Mathematical formulation and examples. *Icarus, 148,* 118–138.
Vokrouhlický D., Brož M., Farinella P., and Knežević Z. (2001) Yarkovsky-driven leakage of Koronis family members. *Icarus, 150,* 78–93.
Welten K. C., Lindner L., van der Borg K., Loeken T., Scherer P., and Schultz L. (1997) Cosmic-ray exposure ages of diogenites and the recent collisional history of the HED parent body/bodies. *Meteoritics & Planet. Sci., 32,* 891–902.
Wetherill G. W. (1974) Solar system sources of meteorites and large meteoroids. *Annu. Rev. Earth Planet. Sci., 2,* 303–331.
Wetherill G. W. (1979) Steady state populations of Apollo-Amor objects. *Icarus, 37,* 96–112.
Wetherill G. W. (1985) Asteroidal source of ordinary chondrites (Meteoritical Society Presidential Address 1984). *Meteoritics, 20,* 1–22.
Whipple F. L. (1950) A comet model. I. The acceleration of Comet Encke. *Astrophys. J., 111,* 375–394.
Wisdom J. (1983) Chaotic behavior and the origin of the 3/1 Kirkwood gap. *Icarus, 56,* 51–74.
Wisdom J. and Holman M. (1991) Symplectic maps for the n-body problem. *Astron. J., 102,* 1528–1538.
Zappalà V. and Cellino A. (2002) A search for the collisional parent bodies of large NEAs. *Icarus,* in press.
Zappalà V., Cellino A., Dell'Oro A., Migliorini F., and Paolicchi P. (1996) Reconstructing the original ejection velocity fields of asteroid families. *Icarus, 124,* 156–180.
Zappalà V., Bendjoya P., Cellino A., Di Martino M., Doressoundiram A., Manara A., and Migliorini F. (2000) Fugitives from the Eos family: First spectroscopic confirmation. *Icarus, 145,* 4–11.